Differential Post Detection Integration Techniques for Robust Code Acquisition

Marco Villanti, Paola Salmi, and Giovanni Emanuele Corazza

Abstract

In this paper, the problem of code acquisition for spread spectrum systems is investigated in the presence of frequency errors. The classic approach of non coherent post detection integration (NCPDI) is contrasted with differential post detection integration (DPDI), presented in two different versions, namely DPDI-Real and DPDI-Abs, respectively suited for fine and large frequency offsets. The differential schemes are characterized thoroughly introducing a novel analytical treatment which is validated by simulations. In order to fairly quantify the potential gains introduced by the differential solutions, specific detector parameters optimization is performed for each scheme. The interesting result is that DPDI significantly outperforms the classic NCPDI approach for large frequency errors, and behaves close to it for small offsets. DPDI can be thus considered as a very robust PDI solution with moderate complexity.

Index Terms

Code acquisition, frequency error, post detection integration, differential techniques, spread spectrum systems

I. Introduction

In recent years, spread spectrum technologies have found extensive commercial exploitation in both communication systems, such as 2G and 3G cellular networks, and navigation systems, as the operational GPS and the up-coming GALILEO systems. The most distinctive feature of spread spectrum transmission is that the signal power spectral density is very low, typically under the noise level, N_0, and in these harsh conditions the initial recovery of the received spreading sequence epoch, identified as code synchronization, becomes one of the most critical design issues. Indeed, the epoch search must be performed

This work was supported in part by the EC FP6-IST MAESTRO project, IST-507023.

in a typically very large uncertainty region and in the presence of unknown carrier parameters, which cannot be estimated prior to code synchronization with sufficient accuracy. As a consequence, phase and frequency errors, induced by oscillators mismatch and Doppler effects, must be taken into account for realistic design. To reduce complexity, code synchronization is usually performed in two steps: *code acquisition*, which reduces the code epoch uncertainty to a fraction of the chip interval, and *code tracking*, which provides fine synchronization. Interestingly, even though the problem of code acquisition for direct sequence spread spectrum systems in the presence of carrier uncertainty is a classic matter, it is still possible to study innovative solutions and derive their corresponding analytical characterization. This is the purpose of this paper.

To aid code acquisition, the uncertainty region is quantized into a finite number of cells (typically 2 per chip), and a test variable is extracted from each cell. The decision can then be taken according to different criteria [1], among which the *MAX* (approximate maximum likelihood) criterion, that selects the cell associated to the maximum test variable, the *TC* (threshold crossing) criterion, that performs the decision on single cells by comparing the test variable to a threshold, and the *MAX/TC* criterion, that is a generalization embodying the *MAX* and the *TC* criteria as particular cases. In this paper, a complete analytical characterization of several detection schemes operating with the *TC* criterion is provided. These results can be utilized as inputs into complete search analysis tools, such as those proposed in [2], [3]. In other words, the focus here is on single cell performance characterization, which can then be used to derive the overall probability of acquisition or the statistical moments of the acquisition time, such as the mean acquisition time.

The key problem that this paper addresses is how to exploit efficiently the intrinsic signal-to-noise ratio (SNR) in extracting the test variables. Let Λ be the code length in number of chips. In the absence of carrier uncertainty, the optimal detector would correlate coherently the received signal and the locally generated code replica over the entire code period, achieving a useful component amplitude proportional to Λ. In the presence of phase uncertainty, the classic Maximum Likelihood (ML) solution leads to an energy detector, with a useful output energy proportional to Λ^2. The problem becomes intriguing when a frequency offset is also present, which in fact is the normal condition in the field. In this case, the output energy becomes proportional to $\Lambda^2 \mathrm{sinc}^2(\delta f \Lambda)$ [4], where δf is the frequency offset normalized to the chip rate. In the worst case, when δf is comparable to $1/\Lambda$, the accumulated energy at the output of the coherent correlator effectively vanishes, banning any possible detection capability. To face this difficulty, an effective countermeasure is to fragment coherent correlation over a set of L sequence segments of M chips. Then, the partial results are properly processed by means of Post Detection Integration (PDI).

Evidently, the overall performance is tightly related to the selection of the best (M,L) couple. A possible criterion, based on the maximization of the SNR at the output of the coherent correlator, is presented in [5], where the CHILD *(Coherent Integration Length Dimensioning) rule* has been derived. Essentially, the coherent integration length should be in the order of $3/(8\delta f)$.

Several PDI schemes are possible. Cartier [6] and Viterbi [4] consider non coherent post detection integration (NCPDI) as shown in figure 1.c, which is the natural extension of the energy detector to the case of frequency uncertainty. NCPDI is widely employed in practical applications [6], [7], but can be outperformed by differential PDI (DPDI) techniques in many significant cases, as will be shown in this paper. In essence, DPDI amounts to summing complex conjugate products of adjacent coherent correlation outputs, and then taking either the absolute value (DPDI-Abs) (see fig. 1.a) or the real part (DPDI-Real) (see fig. 1.b). NCPDI and DPDI are not only robust practical approaches, but they are the fundamental elements of the generalized and average likelihood ratio testing solutions as demonstrated in [8].

Differential detection of spreading sequences has been considered before in [9], [10], [11]. In [9] a particular case of DPDI-Real, limited to $L = 2$, is analyzed. This is one of the first examples of differential detection employed for code acquisition. In [10] DPDI-Abs is considered providing an interesting analytical model obtained by numerical integration of the characteristic function of the decision variable. DPDI-Abs is used in this case to combine contributions coming from the slotted repetitions of a preamble, so the optimization of M and L has not been taken into account. Further, an application of NCPDI and DPDI-Abs to the detection of GPS signals is presented in [11], evaluating performance through simulations.

However, even though DPDI has been studied before, its complete analytical characterization, in terms of closed form performance, and the fair comparison among all options listed above are still open problems. Further, a clear criterion to select the most suitable PDI scheme in a given scenario is not present in the literature. Some preliminary steps on these two issues have been taken in [12] and [13]. In particular, in the former an analytical model for DPDI-Real, alternative to [9], is presented, but it applies only for $L = 2$. In the latter, a numerical comparison between all PDI schemes is presented.

In this paper, a completely new analytical model for DPDI-Real and DPDI-Abs detection performance is introduced. Non-ideal effects such as frequency errors, imperfect sequence autocorrelation properties (self noise), fractional timing errors, and realistic band-limited pulse shapes are taken into account. The analytical results can be used for cross-validation with simulations in the optimized selection of M and L, and to perform trade-offs among the proposed schemes in terms of *missed detection*, P_{md}, and *false*

alarm probabilities, P_{fa}. The comparison between all PDI schemes, using the optimal M and L values leads to novel and interesting results which advance the conclusions reached in [10] and [13].

The remaining sections are organized as follows. In Section II, the received signal is characterized and the post integration alternatives are defined. The coherent correlation phase, common to all schemes, is characterized in section III, while the differential accumulated variable, that requires an ad-hoc analytical approach, is described in Section IV. The false alarm and missed detection probabilities are characterized in Section V and VI, respectively. Numerical results are presented in Section VII, for validation of the model and performance comparisons, and, finally, conclusions are drawn in Section VIII.

II. Received Signal and Post Detection Integration

Code synchronization is achieved by detecting the epoch of a known pseudo-noise sequence that can be transmitted continuously or in bursts. The former case employs a pilot sequence [14], while the latter uses a preamble within a packet, which can be juxtaposed to the data part [15] or separated by a guard time [16]. In all cases, the transmission flow can be segmented into frames. The period of the pilot sequence for continuous transmission is normally equal to the frame length. The general base-band equivalent received signal can be written in the form:

$$r(t) = \sum_{m=-\infty}^{+\infty} s(t - T_F(m)) + n(t) \tag{1}$$

with

$$s(t) = \sqrt{\frac{E_c}{2}} \sum_{k=0}^{L_F-1} a_k \, g(t - kT_c) \tag{2}$$

$$a_k = \begin{cases} c_k & k \in [0, \Lambda - 1] \\ d_k & k \in [\Lambda, L_F - 1] \end{cases} \tag{3}$$

where $s(t)$ represents the useful signal in a frame period, $T_F(m)$ is the m-th frame epoch, L_F is the frame length in number of chips, c_k is a complex chip of the pseudo-noise sequence with $c_k^p = Re\{c_k\} = \pm 1$ and $c_k^q = Im\{c_k\} = \pm 1$, d_k results from the multiplication of the k-th chip of the spreading sequence and of a random data symbol (ticking at the chip rate divided by the spreading factor), Λ is the length of the known sequence, E_c is the complex chip energy, T_c is the chip period, $g(t)$ is the impulse response of a squared root raised cosine filter normalized in energy, $\int_{-\infty}^{+\infty} g^2(t)dt = 1$, and $n(t)$ is the complex additive white Gaussian noise (AWGN) process with double-sided power spectral density N_0.

The above model contains several useful particular cases: a DS-CDMA continuous pilot, characterized by $\Lambda = L_F$ and $T_F(m) = m\Lambda T_c$; TDMA transmission, interpreting chips as symbols, and considering a frame length $L_F > \Lambda$ and a frame period equal to $T_F(m)/m \geq \Lambda T_c$. In this case, the known sequence is the so-called unique word marking the start of frame [5]. In addition, the parameter $T_F(m)$ can be used to include both synchronous and asynchronous packet access.

Considering that the received signal contains unknown delay, frequency, and phase, at the output of the chip matched filter, the in-phase and quadrature components of the signal sampled at time $t_i = iT_c + \tau$, are given by:

$$r_i^{p/q} = \sqrt{\frac{E_c}{2}} \sum_{\ell=-\infty}^{+\infty} (a_{i-\ell}^{p/q} \cos\varphi_i \mp a_{i-\ell}^{q/p} \sin\varphi_i) R_g\big(\ell T_c + \tau\big) + \eta_i^{p/q} \tag{4}$$

where hereafter it is intended that the upper operator in $\mp$ (or $\pm$) refers to the equation specified for the first element in superscript $z^{x/y}$, while the lower operator applies to the second element on the superscript $z^{x/y}$. Further, $R_g(\cdot)$ is the chip pulse autocorrelation function, ℓ and τ are respectively the integer and fractional parts of the delay, with $\tau \in [-\frac{T_c}{2}, \frac{T_c}{2}]$, $\eta_i^{p/q}$ are the in-phase/quadrature samples of the filtered Gaussian noise, with zero-mean and variance $\sigma^2 = N_0/2$. The rotation $\varphi_i = \phi + \omega_s i T_c$ accounts for both the frequency offset Δf (or equivalently the angular frequency offset $\omega_s = 2\pi\Delta f$) and the carrier phase, ϕ. The maximum value of ω_s is a known specification, and is used for a worst-case design. Note that $\ell = 0$ tags the desired contribution, whereas $\ell \neq 0$ represents inter-chip interference (ICI).

As explained in the Introduction, the presence of a frequency error calls for a combination of coherent and post detection integration, respectively over M chips and L segments. Denoting with Δ the code epoch offset of the locally generated sequence with respect to the received signal, the in-phase and quadrature coherent integrator outputs are given by:

$$y_j^{p/q}(\Delta) = x_j^{p/q}(\Delta) + \nu_j^{p/q} = \frac{1}{\sqrt{2}} \sum_{i=jM}^{(j+1)M-1} \Big(r_i^{p/q} c_{|i+\Delta|_\Lambda}^{p/p} \pm r_i^{q/p} c_{|i+\Delta|_\Lambda}^{q/q} \Big) \tag{5}$$

where

$$\begin{aligned} x_j^{p/q}(\Delta) = \frac{\sqrt{E_c}}{2} \sum_{i=jM}^{(j+1)M-1} \sum_{\ell} R_g(\ell T_c + \tau) \cdot \\ \cdot \Big[(a_{i-\ell}^{p/q} c_{|i+\Delta|_\Lambda}^{p/p} \pm a_{i-\ell}^{q/p} c_{|i+\Delta|_\Lambda}^{q/q}) \cos\varphi_i + (a_{i-\ell}^{p/p} c_{|i+\Delta|_\Lambda}^{q/p} \mp a_{i-\ell}^{q/q} c_{|i+\Delta|_\Lambda}^{p/q}) \sin\varphi_i \Big] \end{aligned} \tag{6}$$

and

$$\nu_j^{p/q} = \frac{1}{\sqrt{2}} \sum_{i=jM}^{(j+1)M-1} \Big(\eta_i^{p/q} c_{|i+\Delta|_\Lambda}^{p/p} \pm \eta_i^{q/p} c_{|i+\Delta|_\Lambda}^{q/q} \Big) \tag{7}$$

Note that a factor $\frac{1}{\sqrt{2}}$ is introduced to normalize the local sequence chip energy to one and $|a|_b \triangleq a \bmod b$. Therefore, the term $\nu_j^{p/q}$ is a Gaussian random variable (r.v.) with zero mean and variance $M\sigma^2$. Different values of Δ identify different code epoch hypotheses. The locally generated sequence is correctly aligned if $\Delta = 0$, identified as the H_1 hypothesis, while it is out of sync otherwise, identified as the H_0 hypotheses. Note that to improve the readability of the paper, hereafter $y_j(\Delta) = y_j^p(\Delta) + \jmath\, y_j^q(\Delta)$ will be simply identified as y_j, specifying whether it corresponds to either H_1 or H_0.

Coming to the PDI section, three alternative techniques are considered here: DPDI-Real, DPDI-Abs and NCPDI, respectively depicted in figs.1 (a), (b), and (c). Cross-comparisons and trade-offs among the alternatives are non trivial and will be discussed later. The decision statistics for the three alternative PDI schemes are described as follows.

A. Differential Post Detection Integration-Absolute

$$\lambda = \left| \sum_{j=1}^{L-1} y_j y_{j-1}^* \right|^2 \triangleq |z|^2 \tag{8}$$

where z is the differential accumulated variable (DAV).

B. Differential Post Detection Integration-Real

$$\lambda = Re\left\{ \sum_{j=1}^{L-1} y_j y_{j-1}^* \right\} \triangleq Re\{z\} \tag{9}$$

C. Non-Coherent Post Detection Integration

$$\lambda = \sum_{j=0}^{L-1} \left(Re\{y_j\}^2 + Im\{y_j\}^2 \right) = \sum_{j=0}^{L-1} |y_j|^2 \tag{10}$$

Note that for DPDI-Abs and DPDI-Real, only $L-1$ differential terms are obtained from the L samples. However, the reduced noise enhancement offered by the differential schemes with respect to the non-coherent solution yields a gain that will be quantified in the numerical results.

Adopting the threshold crossing *TC* criterion for the binary detection problem at hand, the testing performance is characterized in terms of missed detection probability, P_{md}, and false alarm probability, P_{fa}, defined as:

$$P_{md} = \int_{-\infty}^{\gamma} p_{\lambda|H_1}(\lambda|H_1) d\lambda \tag{11}$$

$$P_{fa} = \int_{\gamma}^{\infty} p_{\lambda|H_0}(\lambda|H_0) d\lambda \tag{12}$$

where γ is the decision threshold, to be optimized depending on the PDI scheme, and $p_{\lambda|H_1}(\lambda|H_1)$, $p_{\lambda|H_0}(\lambda|H_0)$ are the conditional probability density functions (p.d.f.'s) of the decision variable λ. In

the following, P_{md} and P_{fa} are analytically derived for all three PDI schemes, accounting for the frequency error, the fractional timing offset and pulse shape filtering. With these impairments, the statistical characterization of the decision variable λ of the differential schemes is far from trivial. In fact, the differential terms composing the decision statistics are not statistically independent. For this reason, a two step approach is adopted. The basic idea is firstly to find a closed form expression for P_{md} and P_{fa} conditioned on the samples at the coherent correlator output with even index, y_{2j}. This can be done either in exact form or using approximations detailed in the following. Then, the conditioning is removed either in closed form or by numerical integration. In order to distinguish clearly the different approaches, the expressions for the characteristic probabilities will be specified as $P_{md} = P_{md}(\textit{scheme, method, closure})$ and $P_{fa} = P_{fa}(\textit{scheme, method, closure})$, where the *scheme* can be equal to Abs, Real, or NC; *method* is either A.A (approximation A), A.B (approximation B), or E (Exact); and *closure* is either C (closed form) or N (numerical).

The analytical performance of NCPDI is a known result [4], reported here for completeness.

III. Coherent Integration Output Statistics

Observing eq. (6), when the received code and the local replica are synchronous, that is $\Delta = 0$, then $a_k = c_k$ and the sum of the cross-products for $\ell = 0$ simply becomes $(c_i^p)^2 + (c_i^q)^2 = 2$, while their difference vanishes. For $\ell \neq 0$, a large number of ICI terms is summed, which can be modeled as a Gaussian r.v. by central limit theorem arguments. On the other hand, for $\Delta \neq 0$, $x_j^{p/q}(\Delta)$ is the sum of cross-products between the pseudo-noise sequence and random data. Again, the central limit theorem can be invoked, which becomes accurate for not too small values of M, so that $x_j^{p/q}(\Delta)$ can be characterized as a Gaussian r.v. with mean and variance dependent on the considered hypothesis:

$$H_1: \quad \begin{cases} E[x_j^{p/q}(0)] = \sqrt{E_c} R_g(\tau) \sum\limits_{i=jM}^{(j+1)M-1} \cos(\varphi_i - \psi^{p/q}) \\ Var[x_j^p(0)] = \frac{1}{2} M E_c \sum\limits_{\ell \neq 0} R_g^2(\ell T_c + \tau) \end{cases} \tag{13}$$

where $\psi^p = 0$ and $\psi^q = \pi/2$. The fact that there exists a non-zero variance under H_1 is commonly identified as *self-noise*. The mean value of the complex variable $x_j(0)$ can be expressed in a more compact formula as:

$$\begin{aligned} E[x_j(0)] &= \sqrt{E_c} R_g(\tau) \sum_{i=jM}^{(j+1)M-1} e^{\jmath\varphi_i} = \sqrt{E_c} R_g(\tau) \sum_{i=jM}^{(j+1)M-1} e^{j(\phi + \omega_s i T_c)} \\ &= e^{\jmath\phi} e^{\jmath\omega_s jMT_c} e^{\jmath\omega_s (M-1)T_c/2} \frac{\sin(\omega_s M T_c/2)}{\sin(\omega_s T_c/2)} \overset{\omega_s T_c \ll 1}{\simeq} A\, e^{\jmath(\Theta_0 + \Theta_j + \phi)} \end{aligned} \tag{14}$$

where $A = \sqrt{E_c} M R_g(\tau) \operatorname{sinc}\left(\frac{\omega_s M T_c}{2\pi}\right)$, $\Theta_0 = \frac{\omega_s (M-1) T_c}{2}$, and $\Theta_j = \omega_s j M T_c$.

Under the H_0 hypothesis, the mean value is simply null, and the self-noise is augmented by the $\ell = 0$ term, i.e. the variance of $x_j^{p/q}(\Delta)$ equals $M \frac{E_c}{2} \sum_\ell R_g^2(\ell T_c + \tau)$. Therefore the statistics of the coherent correlator output $y_j = x_j(\Delta) + \nu_j$ are Gaussian with moments summarized as follows:

$$H_1\ (\Delta = 0)\ : \begin{cases} \mu^{p/q}_{y(j)|H_1} = E[y_j^{p/q}] \simeq \sqrt{E_c} M \operatorname{sinc}\left(\frac{\omega_s M T_c}{2\pi}\right) \cos\left(\Theta_0 + \Theta_j + \phi - \psi^{p/q}\right) R_g(\tau) \\ \sigma^2_{y|H_1} = Var[y_j^{p/q}] = Var[x_j^{p/q}(\Delta) + \nu_j^{p/q}(\Delta)] \simeq M \left(\frac{E_c}{2} \sum_{\ell \neq 0} R_g^2(\ell T_c + \tau) + \sigma^2 \right) \end{cases} \tag{15}$$

$$H_0\ (\Delta \neq 0)\ : \begin{cases} \mu^{p/q}_{y(j)|H_0} = E[y_j^{p/q}] = E[x_j^{p/q}(\Delta) + \nu_j^{p/q}(\Delta)] \simeq 0 \\ \sigma^2_{y|H_0} = Var[y_j^{p/q}(\Delta)] \simeq M \left(\frac{E_c}{2} \sum_\ell R_g^2(\ell T_c + \tau) + \sigma^2 \right) \end{cases} \tag{16}$$

IV. Statistical Characterization of the Differential Accumulated Variable

Letting L be an odd number, the terms composing the variable z which involve a sample y_j with even index can be grouped together yielding:

$$z = \sum_{j=1}^{(L-1)/2} (y_{2j} y^*_{2j-1} + y_{2j+1} y^*_{2j}) = \sum_{j=1}^{(L-1)/2} w_j \tag{17}$$

The variable w_j conditioned on y_{2j}, $w_j | y_{2j}$, is the sum of two conditionally statistically independent Gaussian r.v.'s, and is itself Gaussian. The various w_j variables still have some residual mutual correlation to be accounted for, however z is conditionally Gaussian nonetheless. This allows to evaluate the conditional detection performance in closed form. The closure is exact for DPDI-Real for all odd L and for DPDI-Abs with $L = 3$. In the case of DPDI-Abs with $L > 3$, an approximation is necessary due to the w_j residual mutual correlation. In fact, as shown in [17], the pairs $(w_j | y_{2j}, w_{j+1} | y_{2j+2})$ are conditionally independent for each j, but this property does not apply to the pairs $(Re\{w_j | y_{2j}\}, Re\{w_{j+1} | y_{2j}\})$ and ($Im\{w_j | y_{2j}\}$, $Im\{w_{j+1} | y_{2j}\}$), which enter in the DPDI-Abs formulas.

Finally, the proposed approach could be extended also to the case of even L values, however this leads to cumbersome expressions.

A. DAV Mean value

The variable z conditioned on the complex vector of elements with even index, $\bar{y}^e = [y_2, y_{2j}, ..., y_{L-1}]$, results to be Gaussian, $z \sim \mathcal{N}(\mu_{z|\bar{y}^e}, \sigma^2_{z|\bar{y}^e})$ with:

$$\mu_{z|\bar{y}^e} = E\left[\sum_{j=1}^{(L-1)/2} (y_{2j} y^*_{2j-1} + y_{2j+1} y^*_{2j}) \right] = \sum_{j=1}^{(L-1)/2} \left(\mu^*_{y(2j-1)} y_{2j} + \mu_{y(2j+1)} y^*_{2j} \right) \tag{18}$$

Observing eq.(15), straightforward algebra leads to:

$$\mu_{y(2k+1)} = \mu_{y(2k-1)} e^{\jmath\Theta} \tag{19}$$

where $\Theta = 2\omega_s M T_c$ is the differential phase rotation due to the frequency error. Therefore, the term in eq. (18) can be expressed as:

$$\begin{aligned} \mu^*_{y(2j-1)} y_{2j} + \mu_{y(2j+1)} y^*_{2j} &= \mu^*_{y(2j-1)} y_{2j} + \mu_{y(2j-1)} e^{\jmath\Theta} y^*_{2j} = 2e^{\jmath\frac{\Theta}{2}} Re\{\mu^*_{y(2j-1)} y_{2j} e^{-\jmath\frac{\Theta}{2}}\} \qquad (20) \\ &= 2\sqrt{E_c} M \mathrm{sinc}\left(\frac{\omega_s M T_c}{2\pi}\right) e^{\jmath\frac{\Theta}{2}} R_g(\tau) \left[y^p_{2j}\cos(\Theta_0+\Theta_{2j}+\phi) + y^q_{2j}\sin(\Theta_0+\Theta_{2j}+\phi)\right] \end{aligned}$$

from which:

$$\mu_{z|\bar{y}^e} = 2A\, e^{\jmath\frac{\Theta}{2}} \sum_{j=1}^{(L-1)/2} \left[y^p_{2j}\cos(\Theta_0+\Theta_{2j}+\phi) + y^q_{2j}\sin(\Theta_0+\Theta_{2j}+\phi)\right] \tag{21}$$

being $A = \sqrt{E_c} M \mathrm{sinc}(\frac{\omega_s M T_c}{2\pi}) R_g(\tau)$. The mean value of z^p and z^q ($\mu_{z^p|\bar{y}^e}$ and $\mu_{z^q|\bar{y}^e}$, respectively) conditioned on $\bar{y}_e$ is obtained simply by taking the real and imaginary part of eq. (21).

B. DAV Variance

In general, considering N Gaussian r.v.'s, $X_1, ..., X_N$, where $X_n \sim \mathcal{N}(\mu_{X_n}, \sigma^2_{X_n})$, with covariance $\mathcal{K}_{X_n,X_m}$, for $n \neq m$, the variable $Y = \sum_{n=1}^{N} X_n$ results to be a Gaussian r.v., $Y \sim \mathcal{N}(\mu_Y, \sigma^2_Y)$, where:

$$\mu_Y = \sum_{n=1}^{N} \mu_{X_n} \tag{22}$$

$$\sigma^2_Y = \sum_{n=1}^{N} \sigma^2_{X_n} + \sum_{n=1}^{N}\sum_{\substack{m=1 \\ m\neq n}}^{N} \mathcal{K}_{X_n,X_m} \tag{23}$$

In the study case, the covariance of $w^p_j = Re\{w_j\}$ and $w^p_{j+1} = Re\{w_{j+1}\}$ conditioned on the even terms, $\mathcal{K}_{w^p_j, w^p_{j+1}|y_{2j}, y_{2j+2}}$ results to be:

$$\mathcal{K}_{w^p_j, w^p_{j+1}|y_{2j}, y_{2j+2}} = E[Re\{w_j\}Re\{w_{j+1}\}] - \mu_{w^p_j}\mu_{w^p_{j+1}} = \sigma^2_y(y^p_{2j}y^p_{2j+2} + y^q_{2j}y^q_{2j+2}) \tag{24}$$

and

$$\mathcal{K}_{w^p_m, w^p_n|y_{2m}, y_{2n}} \equiv 0 \quad \text{for} \quad m \neq n+1 \tag{25}$$

Similarly, considering $w^q_j = Im\{w_j\}$ and $w^q_{j+1} = Im\{w_{j+1}\}$, it holds:

$$\begin{aligned} \mathcal{K}_{w^q_j, w^q_{j+1}|y_{2j}, y_{2j+2}} &= -\mathcal{K}_{w^p_j, w^p_{j+1}|y_{2j}, y_{2j+2}} = E[Im\{w_j\}Im\{w_{j+1}\}] - \mu_{w^q_j}\mu_{w^q_{j+1}} \\ &= -\sigma^2_y(y^p_{2j}y^p_{2j+2} + y^q_{2j}y^q_{2j+2}) \end{aligned} \tag{26}$$

and

$$\mathcal{K}_{w_m^q,w_n^q|y_{2m},y_{2n}} \equiv 0 \quad \text{for} \quad m \neq n+1 \tag{27}$$

Thus, from eqs. (23), (24), and (25), the variance of the variables z^p and z^q conditioned on $\bar{y}_e$ can be computed as follows:

$$\begin{aligned}\sigma^2_{z^{p/q}|\bar{y}_e} &= \sum_{j=1}^{(L-1)/2} \sigma^2_{w_j^{p/q}|y_{2j}} + 2\sum_{j=1}^{(L-3)/2} \mathcal{K}_{w_j^{p/q}w_{j+1}^{p/q}|y_{2j}y_{2j+2}} \\ &= 2\sigma_y^2\left[\sum_{j=1}^{\frac{L-1}{2}}|y_{2j}|^2 \pm \sum_{j=1}^{\frac{L-3}{2}}(y_{2j}^p y_{2j+2}^p + y_{2j}^q y_{2j+2}^q)\right]\end{aligned} \tag{28}$$

Note that, in general, the in-phase and quadrature variances are different, which leads to hardly tractable forms. However, for $L = 3$, eq. (28) becomes:

$$\sigma^2_{z^{p/q}|\bar{y}_e} = 2\sigma_y^2|y_{2j}|^2 \tag{29}$$

This expression allows to obtain exact formulas for DPDI-Real and DPDI-Abs performance. In order to obtain the DPDI-Abs performance characterization for $L > 3$, two different approximations are possible to equalize the in-phase and quadrature variances:

- *Approximation A*

$$\mathcal{K}_{w_j^p,w_{j+1}^p|y_{2j},y_{2j+2}} = -\mathcal{K}_{w_j^q,w_{j+1}^q|y_{2j},y_{2j+2}} = 0 \tag{30}$$

$$\Rightarrow \qquad \sigma^2_{z^p|\bar{y}_e} = \sigma^2_{z^q|\bar{y}_e} = 2\sigma_y^2 \sum_{j=1}^{(L-1)/2} |y_{2j}|^2 \tag{31}$$

- *Approximation B*

$$\mathcal{K}_{w_j^q,w_{j+1}^q|y_{2j},y_{2j+2}} = \mathcal{K}_{w_j^p,w_{j+1}^p|y_{2j},y_{2j+2}} \tag{32}$$

$$\Rightarrow \qquad \sigma^2_{z^p|\bar{y}_e} = \sigma^2_{z^q|\bar{y}_e} = 2\sigma_y^2\left[\sum_{j=1}^{\frac{L-1}{2}}|y_{2j}|^2 + \sum_{j=1}^{\frac{L-3}{2}}(y_{2j}^p y_{2j+2}^p + y_{2j}^q y_{2j+2}^q)\right] \tag{33}$$

In particular, approx. A leads to a closed form expression of $P_{fa}(Abs, C, A)$, while approx. B leads to a numerical solution that fits the simulation results with very good accuracy.

C. Summary of DAV statistic

Summarizing the results described above, under the hypotheses H_0 and H_1, the variables z_p and z_q conditioned on the $\bar{y}_e$ are Gaussian r.v.'s with mean and variance given by:

$$H_1: \begin{cases} \mu_{z^p|H_1,\bar{y}^e} = 2A\cos(\Theta/2)\sum_{j=1}^{\frac{L-1}{2}}\left[y_{2j}^p\cos(\Theta_0+\Theta_{2j}+\phi)+y_{2j}^q\sin(\Theta_0+\Theta_{2j}+\phi)\right] \\ \mu_{z^q|H_1,\bar{y}^e} = 2A\sin(\Theta/2)\sum_{j=1}^{\frac{L-1}{2}}\left[y_{2j}^p\cos(\Theta_0+\Theta_{2j}+\phi)+y_{2j}^q\sin(\Theta_0+\Theta_{2j}+\phi)\right] \\ \sigma^2_{z^{p/q}|H_1,\bar{y}^e} = \begin{cases} 2\sigma^2_{y|H_1}\left[\sum_{j=1}^{\frac{L-1}{2}}|y_{2j}|^2 \pm \sum_{j=1}^{\frac{L-3}{2}}(y_{2j}^p y_{2j+2}^p + y_{2j}^q y_{2j+2}^q)\right] & Exact \\ 2\sigma^2_{y|H_1}\sum_{j=1}^{\frac{L-1}{2}}|y_{2j}|^2 & Approx.\ A \\ 2\sigma^2_{y|H_1}\left[\sum_{j=1}^{\frac{L-1}{2}}|y_{2j}|^2 + \sum_{j=1}^{\frac{L-3}{2}}(y_{2j}^p y_{2j+2}^p + y_{2j}^q y_{2j+2}^q)\right] & Approx.\ B \end{cases} \end{cases} \tag{34}$$

(35)

$$H_0: \begin{cases} \mu_{z^{p/q}|H_0,\bar{y}^e} \simeq 0 \\ \sigma^2_{z^{p/q}|H_0,\bar{y}^e} = \begin{cases} 2\sigma^2_{y|H_0}\left[\sum_{j=1}^{\frac{L-1}{2}}|y_{2j}|^2 \pm \sum_{j=1}^{\frac{L-3}{2}}(y_{2j}^p y_{2j+2}^p + y_{2j}^q y_{2j+2}^q)\right] & Exact \\ 2\sigma^2_{y|H_0}\sum_{j=1}^{\frac{L-1}{2}}|y_{2j}|^2 & Approx.\ A \\ 2\sigma^2_{y|H_0}\left[\sum_{j=1}^{\frac{L-1}{2}}|y_{2j}|^2 + \sum_{j=1}^{\frac{L-3}{2}}(y_{2j}^p y_{2j+2}^p + y_{2j}^q y_{2j+2}^q)\right] & Approx.\ B \end{cases} \end{cases} \tag{36}$$

V. False Alarm Probability

The false alarm probability P_{fa} is here obtained for all schemes, DPDI-Abs, DPDI-Real and NCPDI.

A. DPDI-Abs false alarm probability

Considering the DPDI-Abs scheme, the decision variable conditioned on the even terms is $\lambda_{|\bar{y}^e} = |z_{|\bar{y}^e}|^2$. As noted previously, for $L > 3$ it holds $\sigma^2_{z^p|H_0,\bar{y}_e} \neq \sigma^2_{z^q|H_1,\bar{y}_e}$ and the probability density function (p.d.f.) of variable the $\lambda_{|\bar{y}^e}$ is not known in closed form. However, both approximations A and B can be used to argument that $\sigma^2_{z^p|H_0,\bar{y}^e} \simeq \sigma^2_{z^q|H_0,\bar{y}^e}$, so that $\lambda_{|\bar{y}^e}$ is approximately distributed as a central chi-square r.v. with two degrees of freedom, $\chi^2_2(0)$.

In particular, a closed form expression can be achieved applying approx. A of eq. (30), i.e. considering the variance of the $\chi^2_2(0)$ r.v. composing variates reported in eq. (36). Then, $P_{fa|\bar{y}_e}(\mathrm{Abs})$ can be expressed

as:

$$P_{fa|\bar{y}_e}(\mathrm{Abs}) = \int_{\gamma}^{\infty} \frac{1}{2\sigma^2_{z^p|H_0,\bar{y}^e}} \exp\left(-\frac{\lambda}{2\sigma^2_{z^p|H_0,\bar{y}^e}}\right) d\lambda = \exp\left(-\frac{\gamma}{2\sigma^2_{z^p|H_0,\bar{y}^e}}\right) \tag{37}$$

¿From eq. (16), y_{2j} are independent and identically distributed complex Gaussian r.v.'s with zero mean. Hence, the unconditional $P_{fa}(\mathrm{Abs,A.A})$ can be obtained as:

$$P_{fa}(\mathrm{Abs,A.A}) = \left(\frac{2}{\sqrt{2\pi\sigma^2_{y|H_0}}}\right)^{L-1} \int_{\mathbb{R}^{+^{L-1}}} e^{-\frac{\gamma}{2\sigma^2_{z^p|H_0,\bar{y}^e}}} e^{-\frac{||\bar{\zeta}||^2}{2\sigma^2_{y|H_0}}} d\bar{\zeta} \tag{38}$$

where $\bar{\zeta} = [\zeta_1, \zeta_2, ...\zeta_j, ...\zeta_{L-1}]$ and ζ_j is the generic variable y_j^p or y_j^q. Even though eq. (38) is a multi-dimensional integral that is quite burdensome to solve, it is possible to achieve a closed form expression by transforming to spherical coordinates in $\mathbb{R}^{+^{L-1}}$:

$$P_{fa}(\mathrm{Abs,A.A}) = \left(\frac{2}{\sqrt{2\pi\sigma^2_{y|H_0}}}\right)^{L-1} \int_0^{\pi/2} f(\bar{\theta}) d\bar{\theta} \int_0^{\infty} e^{-\frac{\gamma}{4\sigma^2_{y|H_0}\rho^2}} e^{-\frac{\rho^2}{2\sigma^2_{y|H_0}}} \rho^{L-2} d\rho \tag{39}$$

where $f(\bar{\theta})\rho^{L-2} = f(\theta_1, \theta_2, \ldots, \theta_{L-2})\rho^{L-2}$ is the Jacobian determinant and is equal to:

$$f(\bar{\theta})\rho^{L-2} = \rho^{L-2} \prod_{n=1}^{L-3} (\sin\theta_n)^{(L-2)-n} \tag{40}$$

The product of the first $L-2$ integrals is given by:

$$\int_0^{\pi/2} \cdots \int_0^{\pi/2} \prod_{n=1}^{L-3} (\sin\theta_n)^{(L-2)-n} d\bar{\theta} = \prod_{n=0}^{L-3} \frac{\sqrt{\pi}\,\Gamma\left(\frac{1+n}{2}\right)}{n\Gamma(\frac{n}{2})} \tag{41}$$

where $\Gamma(\cdot)$ is the Euler Gamma function. Further, it can be proved that:

$$\int_0^{\infty} e^{-\frac{\gamma+2\rho^4}{4\sigma^2_{y|H_0}\rho^2}} \rho^{L-2} d\rho = \left(\sqrt{\frac{\gamma}{2}}\right)^{\frac{L-1}{2}} \mathrm{K}_{\frac{L-1}{2}}\left[\frac{\sqrt{\gamma}}{\sqrt{2}\sigma^2_{y|H_0}}\right] \tag{42}$$

where $K_\nu[\cdot]$ is the modified Bessel function of second kind of ν-th order. Then, the approximate closed form expression for the false alarm probability is

$$P_{fa}(\mathrm{Abs,A.A,C}) = \prod_{n=0}^{L-3} \frac{\sqrt{\pi}\,\Gamma\left(\frac{1+n}{2}\right)}{n\Gamma(\frac{n}{2})} \left(\frac{\sqrt{2\gamma}}{\pi\sigma^2_{y|H_0}}\right)^{\frac{L-1}{2}} \mathrm{K}_{\frac{L-1}{2}}\left[\frac{\sqrt{\gamma}}{\sqrt{2}\sigma^2_{y|H_0}}\right] \tag{43}$$

It is worthwhile noting that eq. (43) does not require any approximation for $L = 3$, resulting in an exact expression given by:

$$P_{fa}(\mathrm{Abs,E,C}) = \frac{\sqrt{\gamma}}{\sqrt{2}\sigma^2_{y|H_0}} \mathrm{K}_1\left[\frac{\sqrt{\gamma}}{\sqrt{2}\sigma^2_{y|H_0}}\right] \tag{44}$$

To the authors' knowledge, both the approximate ($L > 3$) and exact ($L = 3$) closure of P_{fa} are novel results.

As an alternative, from approx. B, a numerical solution of $P_{fa}(\mathrm{Abs,A.B,N})$ can be obtained as:

$$P_{fa}(\mathrm{Abs,A.B,N}) = \left(\frac{1}{\sqrt{2\pi\sigma^2_{y|H_0}}}\right)^{L-1} \int\limits_{\mathbb{R}^{L-1}} e^{-\frac{\gamma}{2\sigma^2_{z^p|H_0,\bar{y}^e}}} e^{-\frac{||\bar{\zeta}||^2}{2\sigma^2_{y|H_0}}} d\bar{\zeta} \tag{45}$$

where $\sigma^2_{z^p|H_0,\bar{y}^e}$ is still given by eq. (36).

B. DPDI-Real false alarm probability

Under H_0, the decision statistics of DPDI-Real conditioned on the even terms vector $\lambda_{|\bar{y}^e} = Re\{z_{|\bar{y}^e}\}$ is a zero-mean Gaussian r.v. with variance $\sigma^2_{\lambda|H_0,\bar{y}^e} = \sigma^2_{z^p|H_0,\bar{y}_e}$. Thus, the conditional false alarm probability, $P_{fa|\bar{y}_e}(\mathrm{Real})$, can be very simply expressed as:

$$P_{fa|\bar{y}_e}(\mathrm{Real}) = \frac{1}{2}\,\mathrm{erfc}\left(\frac{\gamma}{\sqrt{2}\sigma_{\lambda|H_0,\bar{y}^e}}\right) \tag{46}$$

Because in this case $\lambda \in \mathbb{R}$, negative thresholds could also be considered, but they have no practical bearing. Removing the conditioning on $\bar{y}_e$, $P_{fa}(\mathrm{Real,E,N})$ can be expressed as:

$$P_{fa}(\mathrm{Real,E,N}) = \left(\frac{1}{\sqrt{2\pi\sigma^2_{y|H_0}}}\right)^{L-1} \int\limits_{\mathbb{R}^{L-1}} \frac{1}{2}\,\mathrm{erfc}\left(\frac{\gamma}{\sqrt{2}\sigma_{\lambda|H_0,\bar{y}^e}}\right) e^{-\frac{||\bar{\zeta}||^2}{2\sigma^2_{y|H_0}}} d\bar{\zeta} \tag{47}$$

Eq. (47) has to be evaluated numerically, but it is possible to obtain also an approximate closed form expression by exploiting approx. A. In fact, observing that the integrand in (47) is an even-symmetric function of $\bar{\zeta}$, substituting eq. (31) in eq. (47) and transforming to spherical coordinates in $\mathbb{R}^{+^{L-1}}$, it follows:

$$P_{fa}(\mathrm{Real,A.A,C}) = \prod_{n=0}^{L-3} \frac{\sqrt{\pi}\,\Gamma(\frac{n+1}{2})}{n\Gamma(\frac{n}{2})} \frac{1}{2} \left(\frac{2}{\pi\sigma^2_{y|H_0}}\right)^{\frac{L-1}{2}} \int\limits_0^{\infty} \mathrm{erfc}\left(\frac{\gamma}{2\sqrt{\sigma^2_{y|H_0}\rho^2}}\right) e^{-\frac{\rho^2}{2\sigma^2_{y|H_0}}} \rho^{L-2} d\rho \tag{48}$$

Eq.(48) can be integrated by parts by defining:

$$u' = e^{-\frac{\rho^2}{2\sigma^2_{y|H_0}}} \rho^{L-2} \quad \text{and} \quad v = \mathrm{erfc}\left(\frac{\gamma}{2\sqrt{\sigma^2_{y|H_0}\rho^2}}\right)$$

The term u' can again be integrated by parts and by induction it can be shown that:

$$\int e^{-\frac{\rho^2}{2\sigma^2_{y|H_0}}} \rho^{L-2} d\rho = -\frac{\Gamma\left(\frac{L-1}{2}, \frac{\rho^2}{2\sigma^2_{y|H_0}}\right)}{2(2\sigma^2_{y|H_0})^{\frac{L-1}{2}}} = -\frac{(2\sigma^2_{y|H_0})^{\frac{L-1}{2}} e^{-\frac{\rho^2}{2\sigma^2_{y|H_0}}}}{2} \left(\frac{L-3}{2}\right)! \sum_{h=0}^{\frac{L-3}{2}} \frac{1}{h!} \left(\frac{\rho}{\sqrt{2}\sigma_{y|H_0}}\right)^{2h}$$

where $\Gamma(\cdot,\cdot)$ is the incomplete Euler Gamma function. With some algebra, it is possible to achieve the approximate closed-form expression of $P_{fa}(\mathrm{Real},\mathrm{A.A},\mathrm{C})$:

$$P_{fa}(\mathrm{Real},\mathrm{A.A},\mathrm{C}) = \begin{cases} \sqrt{2}\sqrt{\frac{\gamma}{\sqrt{2}\sigma^2_{y|H_0}}}\left(\frac{1}{\sqrt{\pi}}\right)^L 2^{L-3}\left(\frac{L-3}{2}\right)!\prod_{n=0}^{L-3}\frac{\sqrt{\pi}\Gamma(\frac{n+1}{2})}{n\Gamma(\frac{n}{2})}\sum_{h=0}^{\frac{L-3}{2}}\frac{2^{-h}}{h!}\left(\frac{\gamma}{\sqrt{2}\sigma^2_{y|H_0}}\right)^h \mathrm{K}_{h-\frac{1}{2}}\left[\frac{\gamma}{\sqrt{2}\sigma^2_{y|H_0}}\right]; & \gamma \geq 0 \\ 1-\sqrt{2}\sqrt{\frac{|\gamma|}{\sqrt{2}\sigma^2_{y|H_0}}}\left(\frac{1}{\sqrt{\pi}}\right)^L 2^{L-3}\left(\frac{L-3}{2}\right)!\prod_{n=0}^{L-3}\frac{\sqrt{\pi}\Gamma(\frac{n+1}{2})}{n\Gamma(\frac{n}{2})}\sum_{h=0}^{\frac{L-3}{2}}\frac{2^{-h}}{h!}\left(\frac{|\gamma|}{\sqrt{2}\sigma^2_{y|H_0}}\right)^h \mathrm{K}_{h-\frac{1}{2}}\left[\frac{|\gamma|}{\sqrt{2}\sigma^2_{y|H_0}}\right]; & \gamma < 0 \end{cases} \quad (49)$$

Note that eq.(49) becomes exact for $L = 3$, yielding:

$$P_{fa}(\mathrm{Real},\mathrm{E},\mathrm{C}) = \begin{cases} \sqrt{\frac{\gamma}{\sqrt{2}\sigma^2_{y|H_0}}}\frac{1}{\sqrt{2\pi}}\mathrm{K}_{-\frac{1}{2}}\left[\frac{\gamma}{\sqrt{2}\sigma^2_{y|H_0}}\right]; & \gamma \geq 0 \\ 1-\sqrt{\frac{|\gamma|}{\sqrt{2}\sigma^2_{y|H_0}}}\frac{1}{\sqrt{2\pi}}\mathrm{K}_{-\frac{1}{2}}\left[\frac{|\gamma|}{\sqrt{2}\sigma^2_{y|H_0}}\right]; & \gamma < 0 \end{cases} \quad (50)$$

C. NCPDI false alarm probability

The decision variable λ of NCPDI is a central χ square r.v. with $2L$ degrees of freedom $\chi^2_{2L}(0)$ so that:

$$p_{\lambda|H_0}(\lambda) = \frac{\lambda^{L-1}e^{-\frac{\lambda}{2\sigma^2_{y|H_0}}}}{(2\sigma^2_{y|H_0})^L(L-1)!} \qquad \lambda \geq 0 \quad (51)$$

Thus, the *false alarm probability* can be expressed in closed form as [18]:

$$P_{fa}(\mathrm{NC},\mathrm{E},\mathrm{C}) = \int_\gamma^\infty p_{\lambda|H_0}(\lambda|H_0)d\lambda = e^{-\frac{\gamma}{2\sigma^2_{y|H_0}}}\sum_{h=0}^{L-1}\frac{1}{h!}\left(\frac{\gamma}{2\sigma^2_{y|H_0}}\right)^h \quad (52)$$

VI. Missed Detection Probability

Hereafter, the decision statistics under H_1 are characterized for DPDI-Abs, DPDI-Real, and NCPDI, and integrated to obtain the missed detection probability, P_{md}.

A. DPDI-Abs missed detection probability

Employing approx. A or B, the decision variable $\lambda_{|\bar{y}^e}$ can be statistically characterized by a non-central chi-square distribution with 2 degrees of freedom, $\chi^2_2(d)$, with noncentrality parameter $d = |\mu_{z|H_1,\bar{y}_e}|^2$, where $\mu_{z|H_1,\bar{y}_e}$ is given by (21) and variance of composing variates $\sigma^2_{z^p|H_1,\bar{y}_e} = \sigma^2_{z^q|H_1,\bar{y}_e}$, given by eq. (34).

The conditional *missed detection probability*, $P_{md|\bar{y}_e}(\mathrm{Abs})$, can therefore be expressed as:

$$\begin{aligned} P_{md|\bar{y}_e}(\mathrm{Abs}) &= \int_0^\gamma p_{\lambda|H_1,\bar{y}^e}(\lambda)d\lambda = 1 - \int_\gamma^\infty \frac{1}{2\sigma^2_{z^p|H_1,\bar{y}_e}}\exp\left[-\frac{d+\lambda}{2\sigma^2_{z^p|H_1,\bar{y}_e}}\right] I_0\left(\frac{\sqrt{\lambda d}}{\sigma^2_{z^p|H_1,\bar{y}_e}}\right)d\lambda \\ &= 1 - Q_1\left(\frac{\sqrt{d}}{\sigma^2_{z^p|H_1,\bar{y}_e}};\frac{\sqrt{\gamma}}{\sigma^2_{z^p|H_1,\bar{y}_e}}\right) \end{aligned} \quad (53)$$

where $I_0(\cdot)$ is the zero-th order modified Bessel function of the first kind and $Q_1(\cdot)$ is the Marcum Q function. By averaging $P_{md|\bar{y}_e}(\mathrm{Abs})$ with respect to $\bar{y}^e$, the final expression of $P_{md|\bar{y}_e}(\mathrm{Abs})$ becomes:

$$P_{md}(\mathrm{Abs,A,N}) = 1 - \int\limits_{\mathbb{R}^{L-1}} \left(\frac{1}{\sqrt{2\pi\sigma^2_{y|H_1}}} \right)^{L-1} Q_1 \left(\frac{\sqrt{d}}{\sigma_{z^p|H_1,\bar{y}_e}}; \frac{\sqrt{\gamma}}{\sigma^2_{z^p|H_1,\bar{y}_e}} \right) e^{-\frac{||\bar{y}_e - \bar{\mu}^e||^2}{2\sigma^2_{y|H_1}}} d\bar{y}^e \quad (54)$$

where $\bar{\mu}^e = E[\bar{y}_e]$. Eq. (54) can be evaluated numerically. As shown in section VII, $P_{md}(\mathrm{Abs,A.B,N})$, obtained exploiting approx. B, is very accurate, while $P_{md}(\mathrm{Abs,A.A,N})$, that uses approx. A, slightly under-estimates $P_{md}(\mathrm{Abs})$.

B. DPDI-Real missed detection probability

According to equations (9) and (34), $\lambda_{|\bar{y}^e} = Re\{z_{|\bar{y}^e}\} \sim \mathcal{N}\left(\mu_{\lambda|H_1,\bar{y}^e}; \sigma^2_{\lambda|H_1,\bar{y}_e}\right)$, where $\mu_{\lambda|H_1,\bar{y}_e} = \mu_{z^p|H_1,\bar{y}_e}$ and $\sigma^2_{\lambda|H_1,\bar{y}_e} = \sigma^2_{z^p|H_1,\bar{y}_e}$. Note that, differently from the analysis of DPDI-Abs, no approximations are required to achieve the closure for $P_{md|\bar{y}_e}(\mathrm{Real})$, which can be expressed as:

$$P_{md|\bar{y}_e}(\mathrm{Real}) = 1 - \int_{\gamma}^{\infty} \frac{1}{\sqrt{2\pi\sigma^2_{\lambda|H_1,\bar{y}^e}/2}} e^{-\frac{\left(\lambda - \mu_{\lambda|H_1,\bar{y}^e}\right)^2}{\sigma^2_{\lambda|H_1,\bar{y}^e}}} d\lambda = 1 - \frac{1}{2}\,\mathrm{erfc}\left(\frac{\gamma - \mu_{\lambda|H_1,\bar{y}^e}}{\sqrt{2\sigma^2_{\lambda|H_1,\bar{y}^e}}} \right) \quad (55)$$

By averaging $P_{md|\bar{y}_e}(\mathrm{Real})$ with respect to $\bar{y}^e$, the exact expression of $P_{md}(\mathrm{Real,E,N})$ becomes:

$$P_{md}(\mathrm{Real,E,N}) = 1 - \left(\frac{1}{\sqrt{2\pi\sigma^2_{y|H_1}}} \right)^{L-1} \int\limits_{\mathbb{R}^{L-1}} \frac{1}{2}\,\mathrm{erfc}\left(\frac{\gamma - \mu_{\lambda|H_1,\bar{y}^e}}{\sqrt{2\sigma^2_{\lambda|H_1,\bar{y}^e}}} \right) e^{-\frac{||\bar{y}_e - \bar{\mu}^e||^2}{2\sigma^2_{y|H_1}}} d\bar{y}_e \quad (56)$$

C. NCPDI missed detection probability

From equations (10) and (15), the decision variable λ is a non-central chi square r.v. with $2L$ degrees of freedom $\chi^2_{2L}(d)$. The noncentrality parameter d is given by $d = L[(\mu^p_{y|H_1})^2 + (\mu^q_{y|H_1})^2]$. The likelihood function under H_1 is therefore:

$$p_{\lambda|H_1}(\lambda) = \frac{1}{2\sigma^2_{y|H_1}} \left(\frac{\lambda}{\sqrt{d}} \right)^{\frac{L-1}{2}} \exp\left\{ -\frac{\lambda + \sqrt{d}}{2\sigma^2_{y|H_1}} I_{L-1}\left(\frac{\sqrt{\lambda d}}{\sigma^2_{y|H_1}} \right) \right\} \quad (57)$$

where $I_{L-1}(\cdot)$ is the modified Bessel function of the first kind of $(L-1)^{th}$ order. Therefore, $P_{md}(\mathrm{NC,E,C})$ is given by [18]:

$$P_{md}(\mathrm{NC,E,C}) = 1 - Q_L\left(\frac{\sqrt{d}}{\sigma_{y|H_1}}; \frac{\sqrt{\gamma}}{\sigma_{y|H_1}} \right) \quad (58)$$

where $Q_L(a,b)$ is the Generalized Marcum Q-function.

VII. NUMERICAL RESULTS

The aim of this section is threefold. First, the analytical model is validated through simulations; then, M and L are jointly optimized for the different PDI alternatives; finally, the optimal performance of the three schemes is compared for different frequency errors. The performance is assessed considering a QPSK pseudo-noise sequence of length $\Lambda = 4096$ chips, following the W-CDMA (Wideband-CDMA) standard as a reference [16].

The constant false alarm rate (CFAR) criterion has been adopted for threshold design. Accordingly, γ has been normalized as:

$$\gamma_{\text{norm}} = \begin{cases} \frac{\sqrt{2\gamma}}{\sqrt{L}\,M\,\sigma^2_{y|H_0}} & \text{DPDI-Abs} \\ \frac{\gamma}{L\,M\,\sigma^2_{y|H_0}} & \text{DPDI-Real} \\ \frac{\gamma}{L\,M\,\sigma^2_{y|H_0}} & \text{NCPDI} \end{cases} \tag{59}$$

This normalization implies that, for a fixed γ_{norm}, the false alarm is independent of SNR. Three values of the frequency error have been considered: Δf= 500, 2500, and 5000 Hz. For the W-CDMA chip rate $R_c = 3.84$ Mchip/s, the corresponding normalized frequency errors are $\delta f = \Delta f / R_c = 1.3 \cdot 10^{-4}, 6.5 \cdot 10^{-4}$, and $1.3 \cdot 10^{-3}$.

Finally, M and L have been selected under the constraint $M \cdot L \lesssim \Lambda$, because in some cases the (M, L) pair which ensures optimal performance does not cover the entire preamble, but comes short by a few chips, typically one.

A. Analytical Model Validation

In the following, the exact and approximate P_{fa} and P_{md} expressions are validated through simulations, which include the presence of a mis-aligned sequence under H_0, to account for self-noise. The residual timing error τ is considered only in a few cases to quantify the induced performance degradation, but the general trade-off results obtained with $\tau = 0$ hold true also for $\tau \neq 0$.

In fig. 2, $P_{fa}(\text{NC}, \text{E}, \text{C})$, $P_{fa}(\text{Real}, \text{E}, \text{C})$, $P_{fa}(\text{Abs}, \text{E}, \text{C})$, and the respective simulated curves $P_{fa}(\text{NC})$, $P_{fa}(\text{Real})$, $P_{fa}(\text{Abs})$, are presented as a function of γ_{norm} in AWGN with E_c/N_0= -21dB, $M = 1365$, $L = 3$. The agreement between the curves is completely satisfactory, as expected for exact expressions.

In fig. 3, P_{fa} for DPDI-Abs is reported as a function of γ_{norm} for $M = 819, 455$ and $L = 5, 9$, respectively, in AWGN channel with E_c/N_0=-21dB. Closed form analytical curves with approx. A (solid line), $P_{fa}(\text{Abs}, \text{A.A}, \text{C})$, a numerical expression with approx. B (dashed line), $P_{fa}(\text{Abs}, \text{A.B}, \text{N})$, and simulation results (markers), $P_{fa}(\text{Abs})$, are reported. The closed form with approx. A is fairly tight

for $P_{fa}(\mathrm{Abs}) > 10^{-5}$. Differently, approx. B gives an excellent overlapping with simulated results. Obviously, the advantage of $P_{fa}(\mathrm{Abs}, \mathrm{A.A}, \mathrm{C})$ lies in the fact that its evaluation is immediate for any M and L.

In fig. 4 the $P_{fa}(\mathrm{Real}, \mathrm{A.A}, \mathrm{C})$ analytical curves with approx. A and simulation results, $P_{fa}(\mathrm{Real})$, are presented for M = 819, 585, 455 and L = 5, 7, 9 respectively. For L = 5 and M = 819 the exact performance, $P_{fa}(\mathrm{Real}, \mathrm{E}, \mathrm{N})$, obtained numerically evaluating eq. (47) is also shown. As expected, the exact curve is perfectly overlapping with the simulation results. However, the use of approx. A leads to a very tight approximation.

In fig. 5, analytical and simulated P_{md} curves are presented as a function of the normalized threshold, for NCPDI, DPDI-Real, and DPDI-Abs, δf=0 and $\delta f = 1.3 \cdot 10^{-4}$ in AWGN with E_c/N_0=-21dB, $M = 1365$, $L = 3$. Even in this case, the exact analytical model fits perfectly the simulated results.

$P_{md}(\mathrm{Real}, \mathrm{E}, \mathrm{N})$ versus γ_{norm} is reported in fig. 6 with $L = 5$ and $M = 819$, AWGN channel, E_c/N_0=-24,-21dB, $\delta f = 0$ and $\delta f = 1.3 \cdot 10^{-4}$, $\tau = 0$ and $\tau = 0.25$. Numerically evaluated analytical curves (solid lines) and simulation results (markers) are reported. The perfect agreement between the exact analytical model and simulation results can be observed once again.

B. Performance Optimization and Comparison

In the following, the optimization and the performance comparison is presented in terms of receiver operating characteristics (ROCs), for all of the PDI schemes, where P_{md} is reported versus P_{fa}. ROCs allow an immediate fair and direct comparison between different detectors: the best performance is given by the PDI scheme ensuring the most favorable P_{md} for a fixed P_{fa}. For fairness, the coherent correlation length, M, and the PDI length, L, have been optimized for each frequency error. To this purpose, the value of $M = M_{CH}$ obtained employing the CHILD rule [5] has been used as a starting point in the optimization process. More specifically, M_{CH} is given by

$$M_{CH} = \left\lfloor \frac{3}{8\,\delta f} \right\rfloor \tag{60}$$

which assumes the values 2884, 576, 288 for $\delta f = 1.3 \cdot 10^{-4}, 6.5 \cdot 10^{-4}, 1.3 \cdot 10^{-3}$, respectively. Under the constraint $\Lambda = M \cdot L = 4096$ (or 4095), the values $\bar{M}_{CH}$ closer to M_{CH} are 2048 (or 1365), 512 (or 455), 256 (or 273). Larger/smaller values than $\bar{M}_{CH}$ have been tested to assess the optimization process, because the CHILD rule does not take into account the presence of the PDI stage. Hence, the best performance can correspond to a different trade-off between M and L, which however is usually close to the pair ($\bar{M}_{CH}$, $\Lambda/\bar{M}_{CH}$).

In figures 7-9 the ROC in AWGN, E_c/N_0=-21dB, $\delta f = 1.3 \cdot 10^{-4}, 6.5 \cdot 10^{-4}, 1.3 \cdot 10^{-3}$ are reported for DPDI-Abs, DPDI-Real and NCPDI, respectively. The best performance, achieved with optimal M and L, is reported in all figures with dashed lines. In particular, the optimum choice corresponding to $\delta f = 1.3 \cdot 10^{-4}, 6.5 \cdot 10^{-4}, 1.3 \cdot 10^{-3}$ is obtained by respectively adopting $M = 1024, 315, 128$ with DPDI-Abs; $M = 512, 64, 64$ with DPDI-Real and $M = 1365, 409, 128$ with NCPDI.

Finally, fig. 10 contains the trade-off indications which can be used in the design of a practical PDI-based code acquisition scheme. In particular, the optimal performance of each scheme is plotted in all cases. Starting with the trade-off between DPDI-Abs and DPDI-Real, from the figure it can be observed that the former outperforms the latter except for very small frequency errors. Therefore, DPDI-Abs appears to be the more robust solution. The second observation is that in general there exists a crossing point between NCPDI and DPDI-Abs. In particular, DPDI-Abs yields better performance for low P_{fa} values, while NCPDI is preferable for very small P_{md} specifications. The former case is much more interesting for practical applications because in general the number of H_0 cells is orders of magnitude larger than the corresponding number of H_1 cells, therefore it can be concluded that DPDI-Abs is in general more appealing than NCPDI. This becomes more and more true as the frequency error becomes larger. On the other hand, for small frequency errors NCPDI is perfectly adequate.

VIII. Conclusions

In this paper, the problem of code acquisition in the presence of frequency errors has been addressed. Different post detection integration (PDI) techniques have been investigated in depth. In particular, non coherent PDI (NCPDI) and two differential post detection integration options (DPDI-Abs and DPDI-Real) have been analytically characterized. The trade-offs between the various schemes have been carried out with optimized parameters to ensure fairness.

As shown by analysis and simulations, for large frequency errors DPDI-Abs is significantly better than NCPDI and DPDI-Real, while, for small frequency errors, the performance of all detectors is very close, with a limited advantage of NCPDI for large false alarm probabilities. ¿From the schematic block diagram, the complexity of DPDI-Abs is only slightly larger than that of NCPDI, and both can be implemented as matched filters to reduce delay. In general, DPDI-Abs appears to be the most robust scheme for practical use.

References

[1] G.E. Corazza, "On the MAX/TC Criterion for Code Acquisition and Its Application to DS-SSMA Systems," *IEEE Trans. on Comm.*, vol. 44, no. 9, pp. 1173–1182, Sep. 1996.

[2] C. Caini, G.E. Corazza, and A. Vanelli-Coralli, "DS-CDMA Code Acquisition in the Presence of Correlated Fading-Part II: Application to Cellular Networks," *IEEE Trans. on Comm.*, vol. 52, no. 8, pp. 1397–1407, Aug. 2004.

[3] G.E. Corazza, C. Caini, A. Vanelli-Coralli, and A. Polydoros, "DS-CDMA Code Acquisition in the Presence of Correlated Fading-Part I: Theoretical Aspects," *IEEE Trans. on Comm.*, vol. 52, no. 7, pp. 1160–1168, Jul. 2004.

[4] A.J. Viterbi, *CDMA, Principles of Spread Spectrum Communications*, Addison-Wesley Wireless Communications Series. Addison-Wesley Publishing Company, April 1995.

[5] G.E. Corazza, T. Mathiopolous, R. Pedone, and M. Villanti, "Frame Synchronization: Analysis and Design," *to be submitted to IEEE Trans. on Comm.*, 2005.

[6] D.E. Cartier, "Partial Correlation Properties of Pseudonoise(PN) Codes in Noncoeherent Synchrnoization/Detection Schemes," *IEEE Trans. on Comm.*, vol. 24, no. 8, pp. 898–903, Aug. 1976.

[7] R. De Gaudenzi, F. Giannetti, and M. Luise, "Signal Recognition and Signature Code Acquisition in CDMA Mobile Packet Communications," *IEEE Trans. Vehicular Technology.*, pp. 196–208, Feb. 1998.

[8] G.E. Corazza and R. Pedone, "Generalized and Average Likelihood Ratio Testing for Post Detection Integration," *submitted to IEEE Trans. on Comm.*, Dec. 2004.

[9] M. Zarrabizadeh and E. Sousa, "A Differentially Coherent PN Code Acquisition Receiver for CDMA Systems," *IEEE Trans. on Comm.*, vol. 45, pp. 1456–1465, Nov. 1997.

[10] Yeon Kyoon Jeong, Oh-Soon Shin, and Kwang Bok Lee, "Fast Slot Synchronization for Intercell Asynchronous DS/CDMA Systems," *IEEE Trans. on Wireless Comm.*, vol. 1, no. 2, pp. 353–360, Apr. 2002.

[11] Harald Elders-Boll and Uwe Dettmar, "Efficient Differentially Coherent Code/Doppler Acquisition of Weak GPS Signals," *IEEE International Symposium on Spread Spectrum Techniques and Application, ISSSTA2004, Sydney, Australia*, vol. 1, pp. 731–735, 30 Aug. - 2 Sep. 2004.

[12] G.E. Corazza, P. Salmi, A. Vanelli-Coralli, and M. Villanti, "Differential Post Detection Integration Technique in the Return Link of Satellite CDMA Systems," *IEEE International Symposium on Spread Spectrum Techniques and Application, ISSSTA2002, Prague, Czech Republic*, pp. 233–237, Sep. 2002.

[13] G.E. Corazza, P. Salmi, A. Vanelli-Coralli, and M. Villanti, "Differential and Non-Coherent Post Detection Integration Techniques for the Return Link of Satellite W-CDMA Systems," *Personal, Indoor and Mobile Radio Communications, PIMRC2002. The 13th IEEE International Symposium on, Lisboa, Portugal*, vol. 1, pp. 300–304, Sep. 2002.

[14] G. E. Corazza and De Gaudenzi R., "Pilot-Aided Coherent Uplink for Mobile Satellite CDMA Networks," *IEEE Trans. on Comm.*, vol. 47, no. 5, pp. 773–783, May 1999.

[15] ETSI TS 101 851-3, "Satellite component of umts/imt 2000; a-family; part 3: Spreading and modulation (s-umts-a 25.213)," *version V1.1.1*, Dec. 2000.

[16] 3GPP TS 25.213, "3rd generation partnership project; technical specification group radio access network; spreading and modulation (fdd) (release 6)," *version V6.0.0*, Dec. 2003.

[17] M. Villanti, *Advanced Communication Systems for Future Generation Wireless Applications*, Ph.D. thesis, University of Bologna, Mar. 2005.

[18] J. Proakis, *Digital Communications*, Mc-Graw Hill, 2nd ed. edition, 1989.

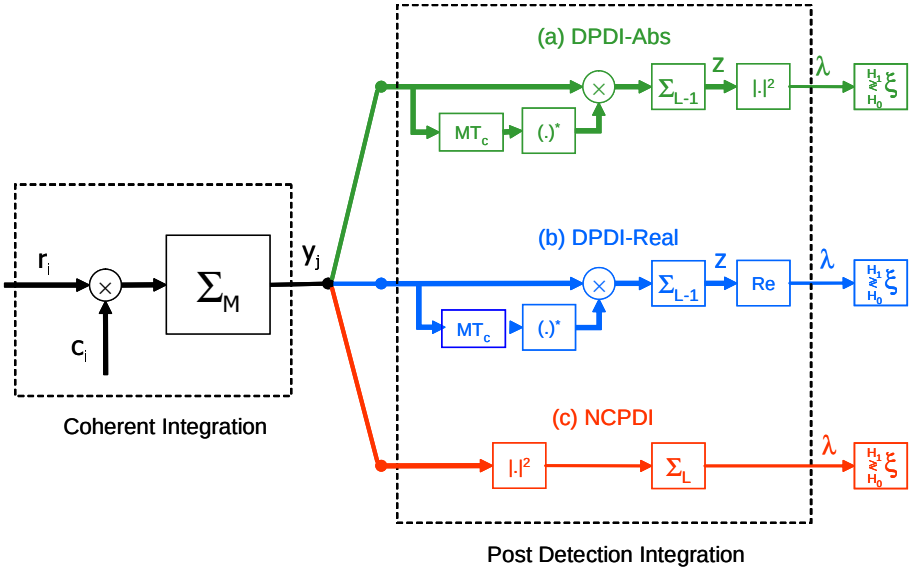

Fig. 1. Post Detection Integration block diagrams: (a) DPDI-Real, (b) DPDI-Abs, (c) NCPDI.

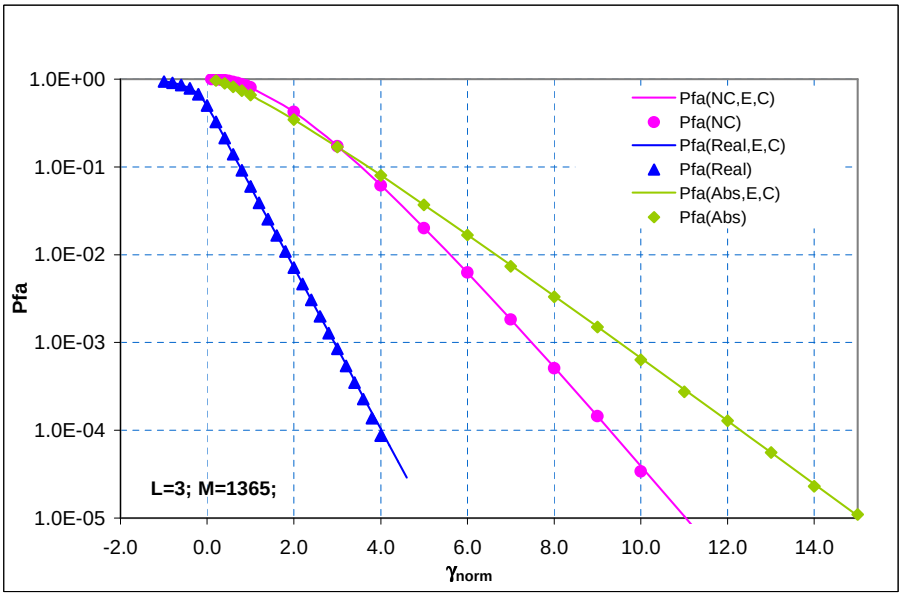

Fig. 2. False alarm probability, P_{fa}, for NCPDI, DPDI-Abs, and DPDI-Real vs. normalized decision threshold, $\gamma_{\rm norm}$, AWGN, E_c/N_0=-21dB, $M = 1365$, $L = 3$, $\tau = 0$. Closed form analytical curves (solid lines) and simulation results (markers) are reported.

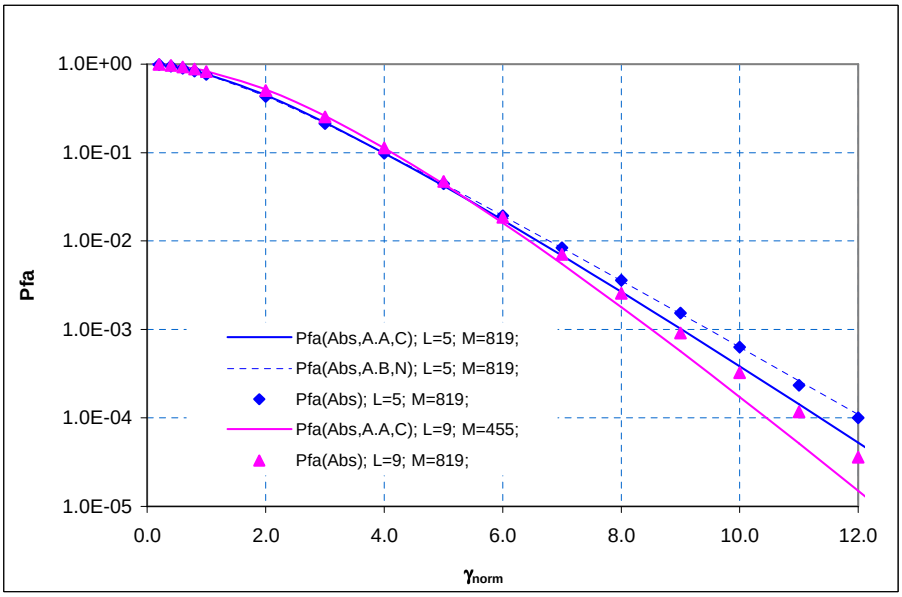

Fig. 3. False alarm probability, P_{fa}, performance vs. normalized decision thresholds, $\gamma_{\rm norm}$, for DPDI-Abs scheme with different values of M and L. AWGN channel, E_c/N_0=-21dB, $\tau = 0$. Closed form analytical curves with *approx A* (solid line), numerical expression with *approx B* (dashed line) and simulation results (markers) are reported.

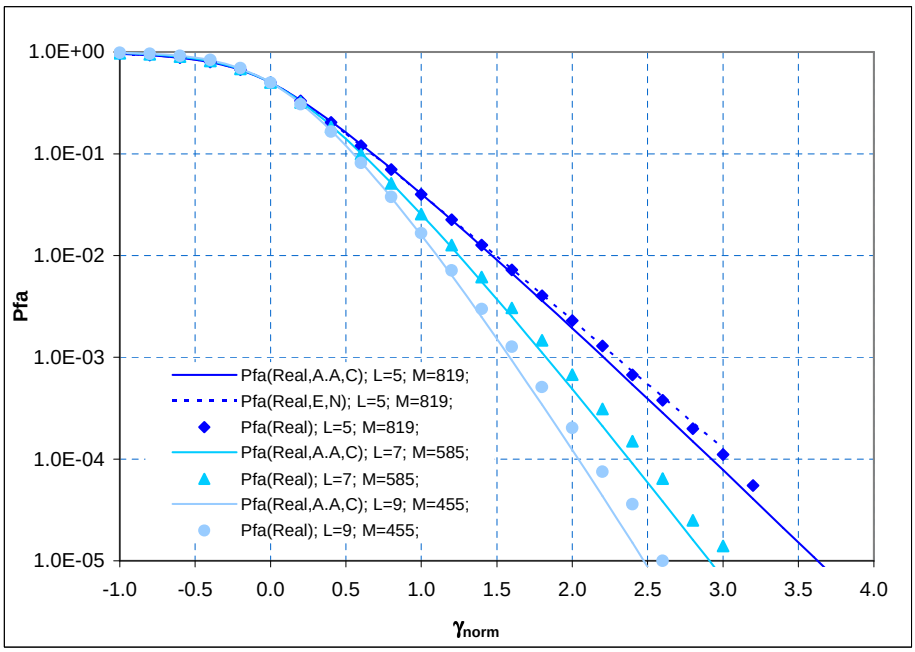

Fig. 4. False alarm probability, P_{fa}, vs. normalized decision thresholds, $\gamma_{\rm norm}$, for DPDI-Real with different values of M and L. AWGN channel, E_c/N_0=-21dB, $\tau = 0$. Closed form analytical curves with *approx A* (solid lines), numerical exact expression (dashed curve) and simulation results (markers) are reported.

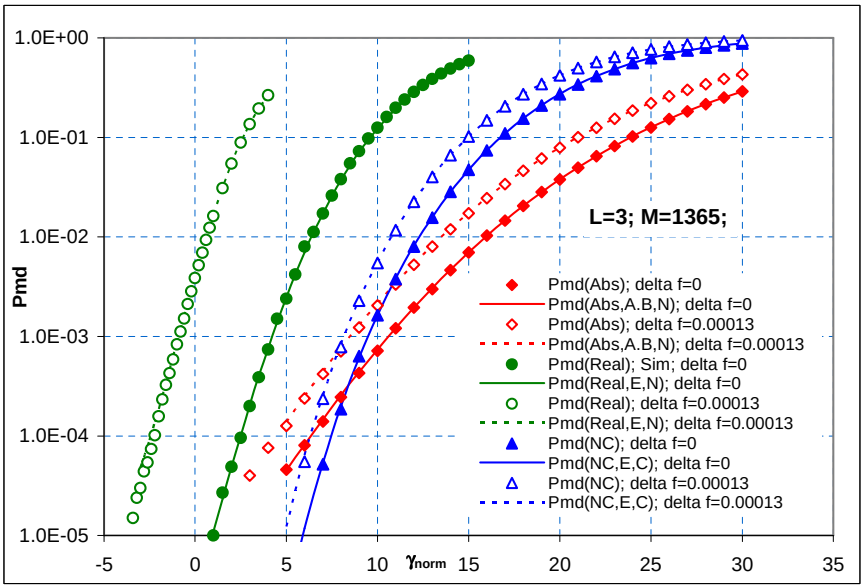

Fig. 5. Missed detection probability, P_{md}, vs. the normalized decision threshold, $\gamma_{\rm norm}$, for NCPDI, DPDI-Abs, and DPDI-Real with L=3, M=1365, for $\delta f = 0$ and $\delta f = 0.00013$. AWGN channel, E_c/N_0=-21dB, $\tau = 0$. Analytical and simulation results are reported.

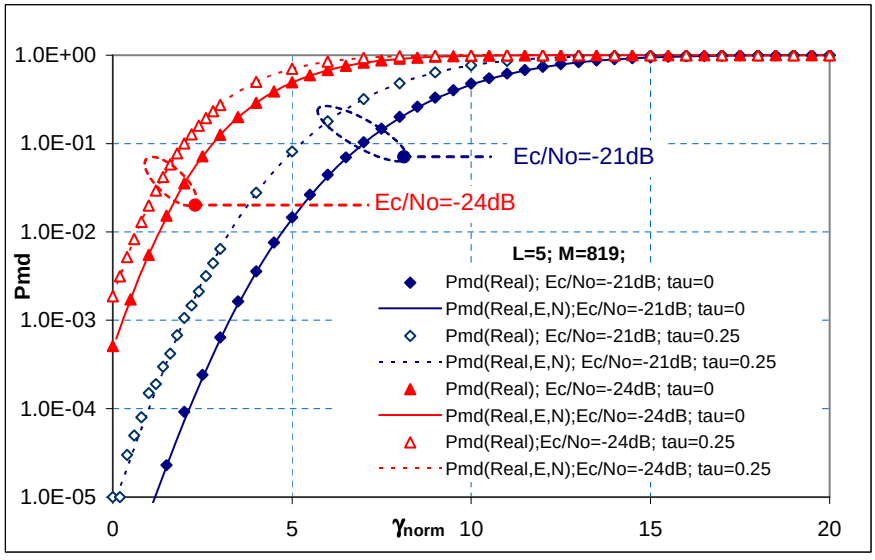

Fig. 6. Missed detection probability, P_{md}, performance vs. normalized threshold, $\gamma_{\rm norm}$, are reported for DPDI-Real with $L = 5$ and $M = 819$. AWGN channel, E_c/N_0=-24,-21dB, $\tau = 0$ and $\tau = 0.25$. Exact numerical curves (solid lines) and simulation results (markers) are reported.

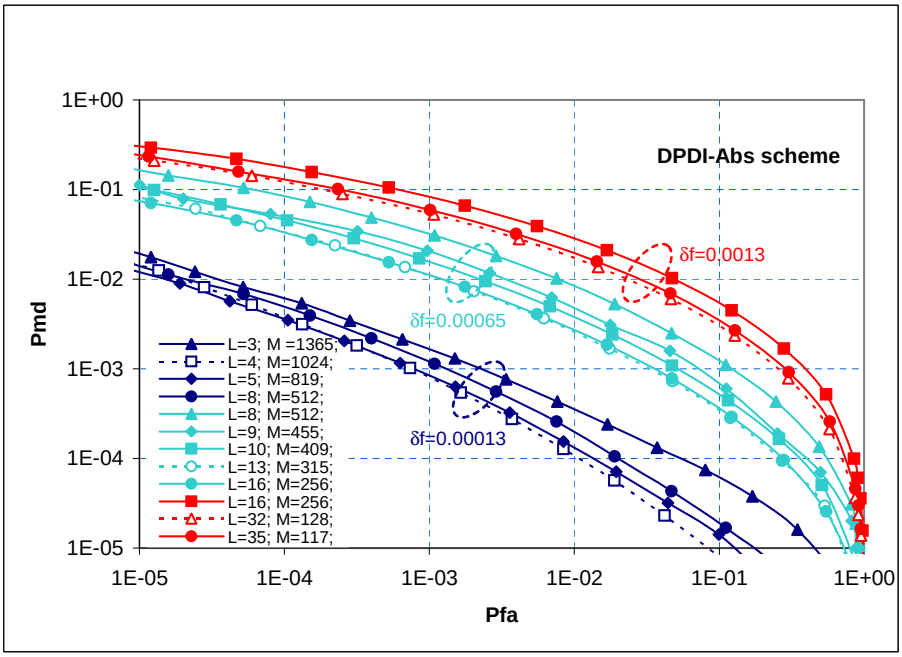

Fig. 7. Simulated P_{md} vs. P_{fa} in AWGN channel, DPDI-Abs, E_c/N_0=-21dB, $\tau = 0$, $\delta f = 1.3 \cdot 10^{-4}, 6.5 \cdot 10^{-4}, 1.3 \cdot 10^{-3}$. Different values of M and L are reported to find the optimum performance at each frequency error.

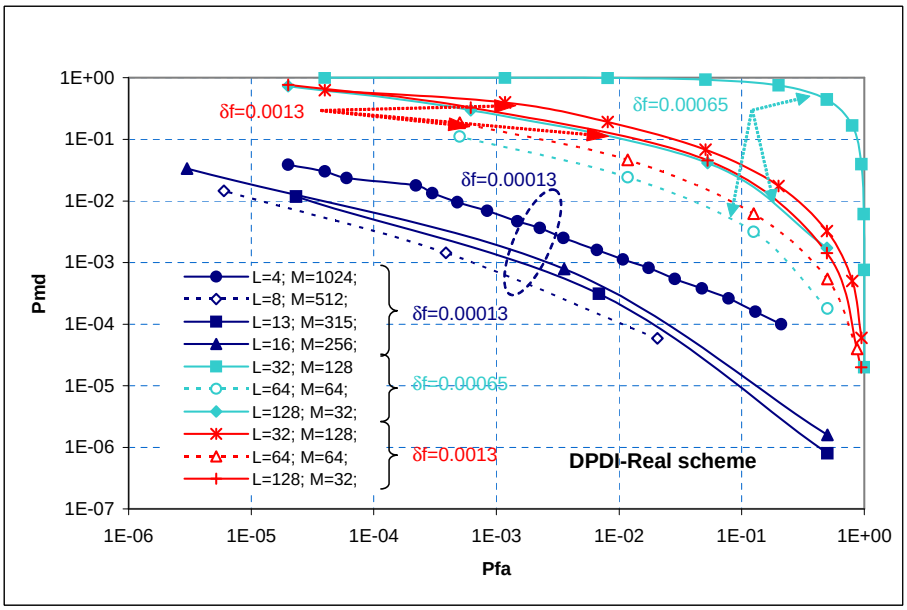

Fig. 8. Simulated P_{md} vs. P_{fa} in AWGN channel, DPDI-Real, E_c/N_0=-21dB, $\tau = 0$, $\delta f = 1.3 \cdot 10^{-4}, 6.5 \cdot 10^{-4}, 1.3 \cdot 10^{-3}$. Different values of M and L are reported to find the optimum performance at each frequency error.

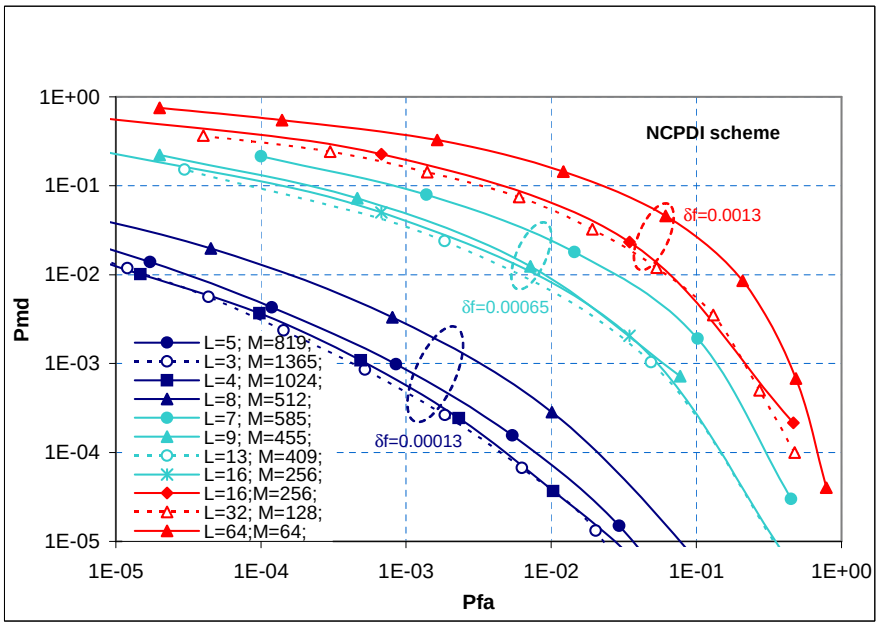

Fig. 9. Simulated P_{md} vs. P_{fa} in AWGN channel, NCPDI, E_c/N_0=-21dB, $\tau = 0$, $\delta f = 1.3 \cdot 10^{-4}, 6.5 \cdot 10^{-4}, 1.3 \cdot 10^{-3}$. Different values of M and L are reported to find the optimum performance at each frequency error.

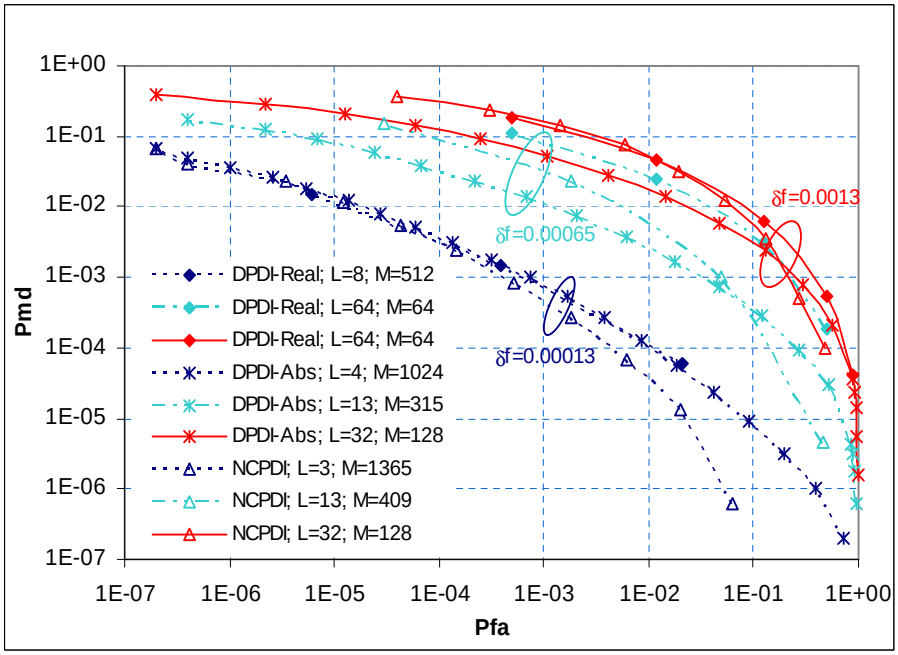

Fig. 10. Performance comparison for DPDI-Abs, DPDI-Real, and NCPDI in AWGN channel, E_c/N_0=-21dB, $\tau = 0$, $\delta f = 1.3 \cdot 10^{-4}, 6.5 \cdot 10^{-4}, 1.3 \cdot 10^{-3}$. The selected values of M and L correspond to the best performance achievable by each scheme.